Proceedings World Geothermal Congress 2023
Beijing, China, April 17 – 21, 2023

Enhancement of geothermal exploitation in Qiabuqia geothermal area using a multilateral horizontal well system

Haizhen Zhai[a], Guangrong Jin[a,*], Lihua Liu[a], Zheng Su[a], Jie Liu[a], Guangyu Li[a,b], Yuchao Zeng[c], Nengyou Wu[d]

a CAS Key Laboratory of Gas Hydrate, Guangzhou Institute of Energy Conversion, Chinese Academy of Sciences, Guangzhou 510640, China

b University of Science and Technology of China, Hefei 230026, China

c Institute of Eco-Environmental and Soil Science, Guangdong Academy of Sciences, Guangzhou 510650, China

d Key Laboratory of Gas Hydrate, Qingdao Institute of Marine Geology, Ministry of Natural Resources, Qingdao 266071, China

zhaihz@ms.giec.ac.cn

Keywords: Hot dry rock; Enhanced geothermal system; Multilateral horizontal well; Power generation; Qiabuqia geothermal area

ABSTRACT

Hot dry rock is one of the most promising clean and renewable energy and can be developed through enhanced geothermal systems (EGSs). The horizontal and multilateral well EGS has potential to achieve a high heat extraction performance of HDR. Herein, multilateral horizontal well system was employed to study the geothermal exploitation performance of the Qiabuqia geothermal area. The exploitation target was selected as the basal granitic reservoir with a depth of 2650 - 3650 m and a corresponding initial temperature of 151 - 190 ℃, based on the geological data of the GR1 borehole. The simulation results indicate that the production temperature reaches 178.4 ℃ and decreases by 8.3% after 20 years under the scheme by injecting 60 ℃ cold water with 50 kg/s rate and a 400 m of lateral well spacing. The energy analysis showed that the designed well system could yield an electric power of 3.58 - 4.35 MW, with the flow impedance of 0.207 - 0.313 MPa/(kg/s) and energy efficiency of 2.7 - 4.5 over a 20 year period. The operation of such a system could reduce the total greenhouse gas (GHG) emissions by 0.21 - 0.72 Mt compared to a fossil fuel plant. The production temperature and electric power of the multilateral horizontal well EGS are higher than those of conventional double vertical wells EGS. The heat production performance of geothermal reservoir highly depends on the well horizon, branch well arrangement, and reservoir permeability. The layout of Lower injection and upper production well is more favorable. A large numbers of branch wells bring the increase of flow impedance and the decrease of production temperature, due to strong well interference. Therefore, under the same total well length, less branches and large spacing between the branch wells is the basic principle for the design of multilateral horizontal well system. A high permeability can effectively reduce flow impedance and save internal energy consumption. The multilateral horizontal well system is a promising development scheme for the geothermal in Qiabuqia geothermal area.

1. INTRODUCTION

1.1 Background

Geothermal energy is one of the most important low-carbon and renewable energy resource alternatives to fossil fuels such as coal, oil and natural gas [1]. Geothermal energy, which utilizes the heat generated in the interior of the earth, is stable and does not rely on weather conditions. Geothermal resources can be divided into hydrothermal geothermal resources and hot dry rock (HDR) geothermal resources, according to the origins and storage conditions. Among them, the reserves of HDR resources are huge and are not limited by region, which is called a new energy that may change the future. The assessment by Wang et al. [2] indicated that the HDR resource within subsurface 3 - 10 km in China could reach 2.09×10^7 EJ. Taking 2% as the recoverable coefficient, the recovered energy is approximately 4400 times of the annual energy consumption of China in 2010 [2].

Due to the low porosity and permeability of the reservoir, it is difficult to exploit and utilize HDR. The enhanced geothermal system (EGS) improves the permeability of the reservoir by constructing artificial thermal reservoir, so as to realize the exploitation of HDR at Fenton Hill in the United States in the early 1970s. During the last few decades, numerous field tests of EGS have been carried out in France (Soultz), Japan (Hijiori), and Australia (Cooper Basin) [3]. In the conventional EGS, two vertical or directional wells are drilled, and one is injection and the other is production well, and an artificial heat reservoir is created by the hydraulic fracturing process.

However, two problems restrict the commercial mining of EGS: 1. the high drilling cost; 2. the stimulation of the artificial heat reservoir is difficult to predict and control. The drilling cost of one 4500 - 5000 m wellbore in EGS is approximately $ 13 - 15 million, which accounts for more than 50% of the total project cost [4]. A large number of artificial thermal reservoir construction experience shows that the generation of artificial fracture network depends on the original in-situ stress and existing fracture system, and the development of new fractures is difficult to predict and control [3]. The geological characteristics of specific areas and the physical properties of reservoir rock mass have a significant impact on the reservoir stimulation results and inter well connectivity, and the portability of reservoir excitation experience in different geothermal fields is poor [3, 5].

Considering of the up two points, scholars proposed horizontal well and multilateral well HDR mining scheme. With these scheme, only one main vertical wellbore is required to be drilled to accomplish injection and production simultaneously, which could significantly reduce the cost compared with the conventional double-well. Moreover, multilateral wells are drilled to increase the contact area of the wellbore and HDR, thereby improving the injectivity and productivity of the wellbore. Meanwhile, the dependence of geothermal development on reservoir stimulation is reduced. Zeng et al. [5] proposed a three horizontal well system to increase

the heat production performance of the Yangbajing geothermal field in Tibet, China. The effects of the key factors, such as thermal conductivity, porosity, and permeability on the performance were studied numerically. Song et al. proposed a novel enhanced geothermal system with multilateral wells for HDR. The results indicated that the output thermal power, production temperature, heat extraction ratio, and the accumulative thermal energy of the multilateral well EGS are higher than those of conventional double vertical wells EGS. Compared to single horizontal well, multilateral horizontal well allow three-dimensional (3D) development and results in a higher production efficiency, and have been widely employed in the petroleum industry [6–8] and unconventional energy recovery [9,10]. Mao et al. [11] constructed a three-dimensional (3D) numerical model of a real gas hydrate reservoir, and the influences of well configuration, deployment location, depressurization pressure, and reservoir properties on production are systemically and quantitatively evaluated. Currently, there are many field applications of multilateral wells in the petroleum industry [12,13] and there is one example for an application in the geothermal energy development. In 2008, 12 multilateral wells with a length of approximately 40 m were side-tracked using the radial jetting technology from an injection well at Klaipėda geothermal field to obtain an improvement in injectivity of approximately 14% [14]. Hence, the horizontal and multilateral well EGS has potential for achieving high heat extraction performance in HDR development.

1.2 Overview of the study area

Gonghe basin is a rhombic Intermountain basin distributed in NWW direction, located between Kunlun Mountains and Qinling Mountains. The tectonic unit belongs to the joint of the East Kunlun and the West Qinling orogenic belt of the Qin-Qi-Kun fault fold system. According to geophysical survey [15], the Gonghe basin can be divided into the Tanggemu depression, Guinan depression, Guide depression, Qijia uplift, and Yellow River uplift (Fig. 1A). The Qiabuqia geothermal area (Fig. 1B) is located in the transition zone of the Tanggemu depression and Yellow River uplift. The average geothermal gradient of granitic formation in this region is greater than 40℃/km [16]. The high geothermal gradient may be caused by the joint effect of high regional background heat flow of the northeastern Tibetan Plateau and the cooling of a shallow magma chamber [17].

Six deep geothermal boreholes (DR1-4, and GR1-2) were drilled in the Qiabuqia geothermal area (Fig. 1B), by China Geological Survey and Land and Resources Department of Qinghai Province since 2013. The DR3, DR4, GR1 and GR2 boreholes are the primary exploration wells for the HDR geothermal resource. The shut-in time of these three boreholes (DR3, DR4 and GR2) before temperature logs are relatively short. The maximum duration between the cessation of drilling and the temperature measurement is less than one month. Considering the effects of drilling-induced thermal perturbation and the circulation of drilling mud, it is inferred that temperature is not fully recovers [18, 19], and the obtained temperature data cannot represent the true static formation temperature (SFT).

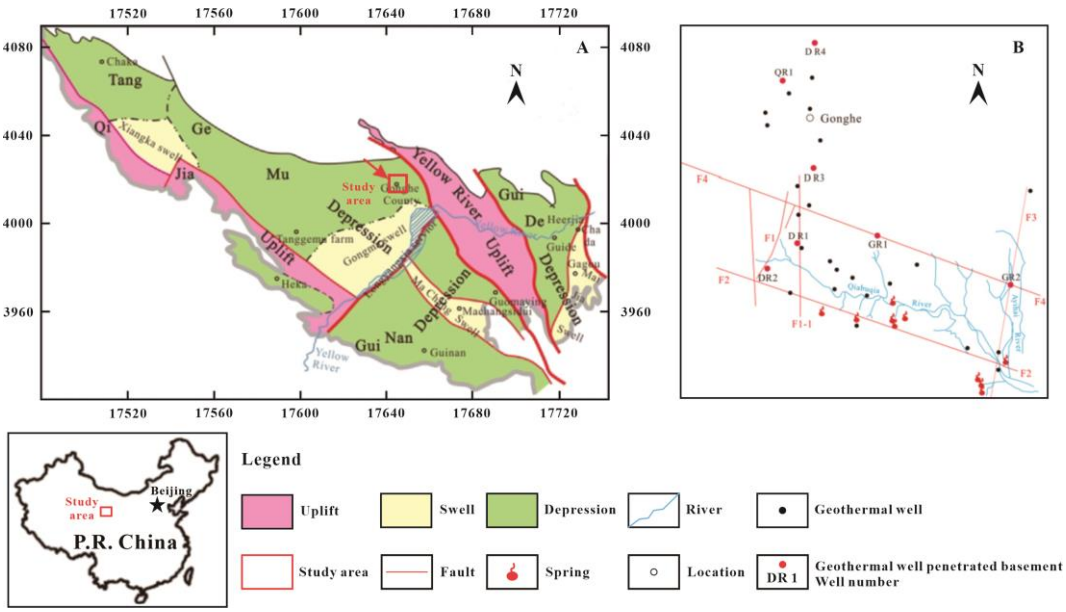

Figure 1: (A) Tectonic map of the Gonghe basin and its neighboring region and (B) wells, springs, and fracture zones distributed in the Qiabuqia geothermal area.

Given the thermal recovery process of borehole since shut-in, the temperature of the GR1 borehole has been measured twice. The first temperature logging was conducted on March 15, 2017, and the second was carried out on May 4, 2018. The duration between the cessation of drilling and the second temperature logging exceeded one year. The two continuous temperature profiles are shown in Fig. 2 for comparison. Based on the two temperature data, the Horner method [21] was applied for computing the SFT. The correction result shows that the corrected data basically coincided with the second temperature data and the discrepancy is less than 0.2 ℃. This indicates that the second logged temperature of GR1 have equilibrated and can be regarded as the steady-state temperature before drilling.

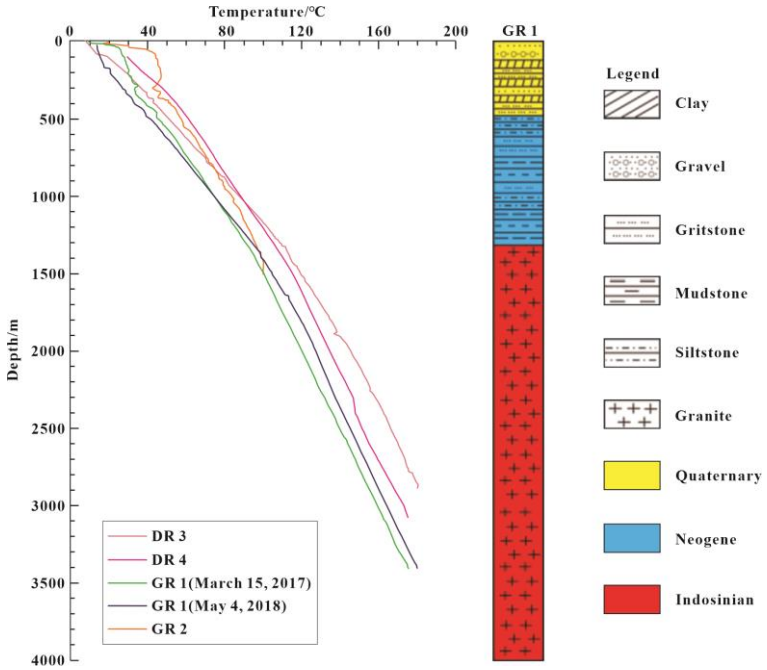

Figure 2: Temperature versus depth plots of DR3, DR4, GR2, and GR1 geothermal wells and the stratigraphic structure revealed by well GR1 in the Qiabuqia geothermal area.

There are three reservoirs in the Qiabuqia geothermal area. Two shallow thermal reservoirs developed in sedimentary cap layer: the Lower Pleistocene reservoir at 100 - 200 m depth and the Neogene reservoir at 667 - 718 m depth [22]. The third thermal reservoir, which appeared below the depth of 1400 m, is mainly impermeable Indosinian granite (Fig. 2). The reservoir temperature at the depth of 2614 m and 3404 m reaches 150 ℃ and 180.6 ℃ respectively. The granitic HDR reservoir has an average geothermal gradient of 41.2 ± 2.96 ℃/km.

With the progress of geothermal exploration and the enrichment of site data, the numerical simulation of Gonghe basin is becoming increasingly. Based on the geological conditions of Qiabuqia area in Gonghe basin, Yue et al. [23] characterized the hydrothermal features of EGS and researched numerically the temporal and spatial distributions of the temperature and pressure fields. The influence of injection temperature and flow rate on heat extraction rate was also analyzed. Xu et al [24] proposed two horizontal wells for the Gonghe Basin using the local thermal non-equilibrium theory (LTNE) and evaluated the production temperature, energy efficiency, and economic and environmental benefits. The numerical results indicated that the electric power mainly depends on fracture spacing and injection temperature, and the saving in greenhouse gas (GHG) emissions ranged between 0.27 and 0.92 Mt over 30 years. Zhang et al [25] established a 3D thermo-hydraulic model to evaluate the performance for the Qiabuqia geothermal area based on the GR1 borehole, and given sensitive parameters that affect electric power output and the optimal combination. A further study based on local thermal non-equilibrium theory and the occurrence of the natural fault indicated that the fault-fracture-controlled doublet model is more suitable for EGS to heat transfer than the common doublet model [26].

1.3 Objective

This paper aims to set up a concept model with a novel multilateral horizontal well system of the deep HDR reservoir of the Qiabuqia geothermal area. The multilateral horizontal well system consist of horizontal wells with one for injection and another for production, with several branches. The well system is applied in the reservoir composed of an HDR layer and a simulated reservoir volume (SRV). The production characteristics of the novel geothermal well system are first investigated. Subsequently, the heat extraction performance between the multilateral horizontal well and several classic double wells are compared. The sensitivity of production criteria to the well horizon, branch number, branch spacing, and permeability of SRV are systematically and quantitatively compared. This study can lay the foundations for the future EGS development with multilateral horizontal well systems at the Qiabuqia geothermal area.

2. DESCRIPTION OF THE NUMERICAL MODEL

2.1 Simulation code

The TOUGH2-EOS1 codes was employed to solve the mathematical models regarding the geothermal heat flow and mass transfer [27]. TOUGH2-EOS1 could model the non-isothermal transport of water, which may exist as aqueous and gas phases according to the conditions of temperature and pressure. The effect of temperature and pressure on physical properties of water and specific enthalpy etc. are built-in the code. TOUGH2 have been validated through experimental results and analytical solution and widely used to evaluate the heat extraction of most geothermal fields [5,23,24]. Specific introductions and governing equations can be found in the user manual and the literature [27].

2.2 Computational model

A multilateral horizontal well EGS model was proposed to develop geothermal energy of the Qiabuqia geothermal area. The geometrical and physical properties of the reservoir are referenced from previous numerical studies [23-26]. The computational

domain comprises an HDR layer enclosing the SRV (Fig. 3). The computational domain is a 1000 m × 1000 m × 1000 m cube with a depth range of 2650 – 3650 m. The SRV is a 500 m × 500 m × 500 m cubic volume and located in the center of the HDR layer. The domain is large enough to reduce the boundary effects during the heat extraction period of interest, which is proved in spatial distribution of temperature in subsequent section. As shown in Fig. 3, the base deployment of multilateral well consists of one horizontal injection well, one horizontal production well, and several branch wells connected to them. The angle between the main horizontal well and the branch well is 90° and the vertical distance between the upper injection well and the lower production well is 400 m. The injection and production wells is 50 m below the top of the SRV and 50 m above the bottom of the SRV. The key geometrical parameters and reservoir properties are listed in Table 1-3, respectively.

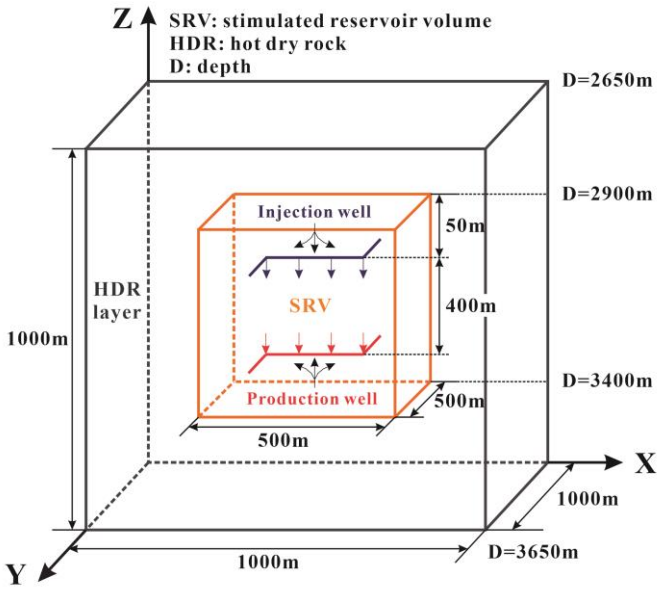

Figure 3: Schematic of the conceptual domain

Considering the highly varying scales between the rock matrix, SRV, and injection and production wells, a Voronoi based un-structure mesh is need to discretize the whole computational domain. The mesh of the SRV and near wellbore were refined. The interfaces between the SRV and the top and bottom HDR are also refined (Fig. 4). The number of mesh in each layer of the base case is 3374. A total of 72 layers was discretized, and therefore the total number of mesh is 242928.

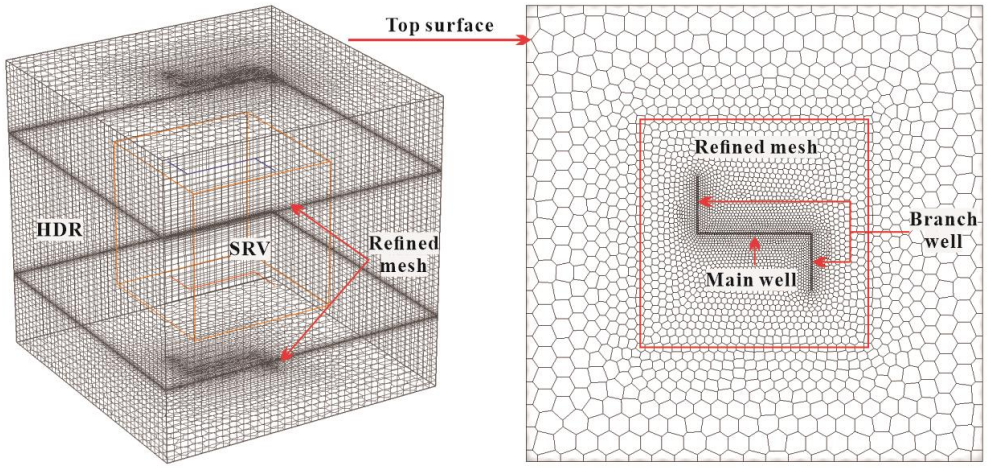

Figure 4: Numerical meshing schemes of the base case.

Table 1 Geometrical parameters of the basic multilateral horizontal model.

Parameters	Values
Computational dimensions	1000 m × 1000 m × 1000 m
SRV dimensions	500 m × 500 m × 500 m
Length of main horizontal wellbore	250 m
Total length of horizontal lateral wells	500 m

Number of branch wells	2
Branch well length	125 m
Branch well spacing	250 m
Well radius	0.1 m
Injection and production well spacing	400 m
Productivity index, PI	8.18×10^{-12} m^3

2.3 Physical properties

Sufficient deep granitic rock samples were recovered from the drilled HDR boreholes in the Qiabuqia geothermal area . The thermal conductivities, densities, and heat capacities of the granite cores from the depth 2900 - 3400 m were measured [25]. For thermal conductivity measured by the Thermal Conductivity Scanning (TCS, manufactured by Lippmann and Rauen GbR Company) with optical scanning technology [28]. The permeability of the granitic rock matrix was measured by the Three Axis MTS Rock Stiff Test Machine [29], while the porosity of reservoir rock was inferred from logging data [30]. The detailed material properties used in the model were listed in Table 2.

Table 2 Reservoir properties of the model.

Parameter	HDR layer	SRV	Wellbore
Density (kg/m^3)	2652	2500	1200
Thermal conductivity (W/(m·K))	2.43	2.8	2.5
Heat capacity (J/(kg·K))	1100	900	750
Porosity (%)	3	10	100
Permeability (m^2)	2.8×10^{-18}	5.0×10^{-15}	1.0×10^{-11}

2.4 Initial and boundary conditions

The initial reservoir pressure is computed according to the relationship between pressure P (MPa) and depth z (m) as according Eq. (1) [5]. The initial reservoir pressure at the top and the bottom of model is 23.5 MPa and 33.5 MPa, respectively.

$$P = -0.0089\ \text{MPa/m} \times z - 0.4444\ \text{MPa} \quad (1)$$

The steady-state temperature profile of the GR1 borehole (Fig. 2) is employed to define the initial temperature distribution of the EGS model, which is defined according to Eq. (2). The initial temperature at the top and bottom of model is 151 ℃ and 190 ℃, respectively.

$$T = 151\ ℃ + 0.0391\ ℃/\text{m} \times (-z - 2650)\ \text{m} \quad (2)$$

where the 151 ℃ is the temperature of the top surface of the computational domain, 39.1 ℃/km is the temperature gradient along the z direction. The equation was acquired by the linear least squares regression method using measured temperature of the depth of 2650 - 3650 m, and the correlation coefficient (R^2) is 0.999.

For the injection well, Dirichlet boundary conditions of 60 ℃ and 50 kg/s, which is a commercial standard mass flow rate for a two well extraction system [31,32], is applied. While an initial pumping mass flow rate of 50 kg/s were applied at the production well. That means the water loss of the modeled domain was neglected in this study. To avoid the boundary effect, the lateral, top, and bottom boundaries were set far away from injection/production wells, these adiabatic and impermeable boundary conditions are assumed insignificant the modeling results.

2.5 Simulation cases

To optimize heat extraction in Qiabuqia geothermal field, the simulation cases designed in this study are listed in Table 4. The simulation scenarios include a base case of 2 branch horizontal well system, several classic double-well system, and other deployments of multi-lateral well system. The scenarios of several classic double well system were designed to verify the reliability and superiority of the 2 branch horizontal well system. Cases 1 and 2 are horizontal double-well EGS with the well length of 250 m and 500 m, which is equal to the horizontal main wellbore length and the total length of multilateral wells respectively. Case 3 is a vertical double-well EGS with one for injection and another for production. The well diameter is 0.1 m and the well spacing is 400 m. The well length is 500 m, which is equal to the total length of multilateral wells. Case 4 reverses the horizon of injection and production well to investigate the effect of well horizon on heat extraction performance. The scenarios of the multilateral well system were designed to investigate the effect of branch number on heat extraction performance. The total length of the branch well is equal

to that of the base case, and cases with 3, 4, 5, 6 branches are set respectively. The length of each branch section is equal, and it is arranged in the direction of cross at equal spacing of the main wellbore. Cases 9 and 10 are designed to investigate the effect of branch spacing on heat extraction performance. Cases 11 and 12 are designed to investigate the effect of permeability of SRV on heat extraction performance.

Table 3 Simulation cases.

Case ID	Well type	Main wellbore length	Well horizon	Branch number	Branch length	Branch spacing	Permeability of SRV	Remark
Base case	Horizontal	250 m	UILP	2	125 m	250 m	5×10^{-15} m^2	Base case
Case 1				-	-	-		Classic double-well EGS
Case 2		500 m		-	-	-		
Case 3	Vertical	500 m	-	-	-	-		
Case 4	Horizontal	250 m	LIUP	2	125 m	250 m	5×10^{-15} m^2	Well horizon
Case 5			UILP	3	83.3 m	125 m		Branch number
Case 6				4	62.5 m	83.3 m		
Case 7				5	50 m	62.5 m		
Case 8				6	41.7 m	50 m		
Case 9				2	125 m	83.3 m		Branch spacing
Case 10						0 m		
Case 11						250 m	1×10^{-15} m^2	Permeability of SRV
Case 12							5×10^{-14} m^2	

where UILP is upper injection lower production, LIUP is lower injection upper production.

2.6 Performance criteria

Several parameters, namely, production temperature, electric power, flow impedance, and electric energy efficiency were defined to characterize the heat performance of different simulation cases.

The production temperature (T_{pro}) is given by

$$T_{\mathrm{pro}} = \frac{\sum T_i q_i}{q} \tag{3}$$

where q_i (kg/s) denotes the mass flow rate for production well of element i, T_i (℃) is the water temperature for production well of element i, and q (kg/s) is the total mass flow rate of the working fluid.

For a geothermal energy exploitation system, the output thermal power (W_{h}) can be calculated by

$$W_{\mathrm{h}} = q c_{p,\mathrm{f}} \left(T_{\mathrm{pro}} - T_{\mathrm{inj}} \right) \tag{4}$$

where T_{inj} is the temperature of the injected water and is 60 ℃, $c_{p,\mathrm{f}}$ is the heat capacity of water. The variation of $c_{p,\mathrm{f}}$ is ignored and an average value of 4200 J/(kg·K) is adopted.

The electric power (W_{e}) can be expressed as

$$W_{\mathrm{e}} = 0.45 \left(1 - \frac{T_{\mathrm{rej}}}{T_{\mathrm{pro}}} \right) W_{\mathrm{h}} \tag{5}$$

where T_{rej} is the heat rejection temperature of water and (T_{rej} / T_{pro}) is calculated with absolute temperature. The mean annual temperature in the Gonghe Basin is 4.1 ℃ [33], thus the heat rejection temperature of 277.25 K is used for electric power calculation. The 0.45 is the utilization efficiency of the maximum mechanical work transferred to electric power [34].

The flow impedance I_R, a key operation parameter for the EGS, represents the power consumption of unit production rate for penetrating fluid through the fractured reservoir, which is defined as [35,36].

$$I_R = (P_{inj} - P_{pro}) / q \tag{6}$$

The bottom-hole pressure of the production well is maintained at 15 MPa. The pressure near the injection well varies due to the constant rate cold water injection, which results in the increase of I_R.

The energy efficiency (η) of the system is defined as the ratio of the total produced thermal energy to the internal energy consumption [36]. The internal energy consumption $W_p = W_{p,inj} + W_{p,pro}$, includes mainly the energy consumed by the injection pumps $W_{p,inj}$ and the production pumps $W_{p,pro}$:

$$W_{p,inj} = q(P_{inj} - \rho g h_{inj}) / \rho \eta_p \tag{7}$$

$$W_{p,pro} = q(\rho g h_{pro} - P_{pro}) / \rho \eta_p \tag{8}$$

In this work, h_{inj}=2950 m, h_{pro}=3350 m, and η_p is pump efficiency and is 80%. The variation of ρ is ignored and an average value of 914 kg/m^3 is adopted. The heat energy efficiency (η_h) based on the heat production rate is calculated from Eq. (9), and the electric energy efficiency (η_e) based on the electric power is calculated from Eq. (10):

$$\eta_h = \frac{W_h}{W_p} = \frac{\rho \eta_p c_{p,f} (T_{pro} - T_{inj})}{(P_{inj} - P_{pro}) - \rho g (h_{inj} - h_{pro})} \tag{9}$$

$$\eta_e = \frac{W_e}{W_p} = \frac{0.45 \rho \eta_p c_{p,f} (T_{pro} - T_{inj})(1 - T_{rej} / T_{pro})}{(P_{inj} - P_{pro}) - \rho g (h_{inj} - h_{pro})} \tag{10}$$

The accumulative energy consumption of pumps (γ_p) can be expressed as

$$\gamma_p = \int_0^t W_p dt \tag{11}$$

3. THE BASE CASE

3.1 Production temperature

Fig. 5 shows the evolution of production temperature (T_{pro}) during a period of 20 years. It can be observed that the production temperature (T_{pro}) of the base case decreases gradually with time. The initial high temperature water is produced due to the initial high temperature of rock near the lower production well caused by the geothermal gradient. The working fluid flows from the upper injection well into the lower production well and is heated up by the rock during the displacement of the hot water. Therefore, the working fluid cannot reach the initial temperature of the rock near the production wells (Fig. 6). As the heat extraction process continues, the cold front propagates downward and reaches the production well, resulting in the continue decrease of the production temperature. According to Garnish et al. (1985), the drop of T_{pro} of an economical EGS for operation life of 15-20 years should be less than 10% [37]. The modeling result indicates that T_{pro} during 20-year drops only 8.3%, and the designed multilateral horizontal well system can meet the temperature requirement of an economical EGS.

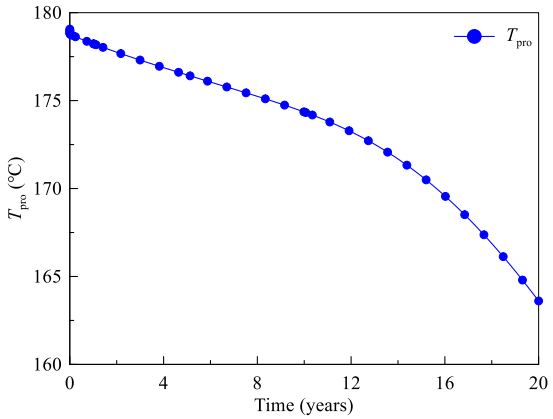

Figure 5: Evolution of production temperature (T_{pro}) of base case.

The evolution pattern of T_{pro} are related to the evolution of fluid temperature in the reservoir. As shown in Fig. 6, the cold region expands gradually with time. The cold region is mainly developed around the injection wellbore, the temperature around the production wellbore decreases little before thermal breakthrough. This is due to the displacement of the water between the well. The

initial temperature of the water between the wells is lower than that of the initial temperature near the well. The cold front expands slowly toward the production well. After about 13 years, the cold front reaches the production well, leading to a faster decrease of the production temperature (Fig. 5). The influence range of pressure drop is larger than that of the temperature because of the faster propagation of pressure.

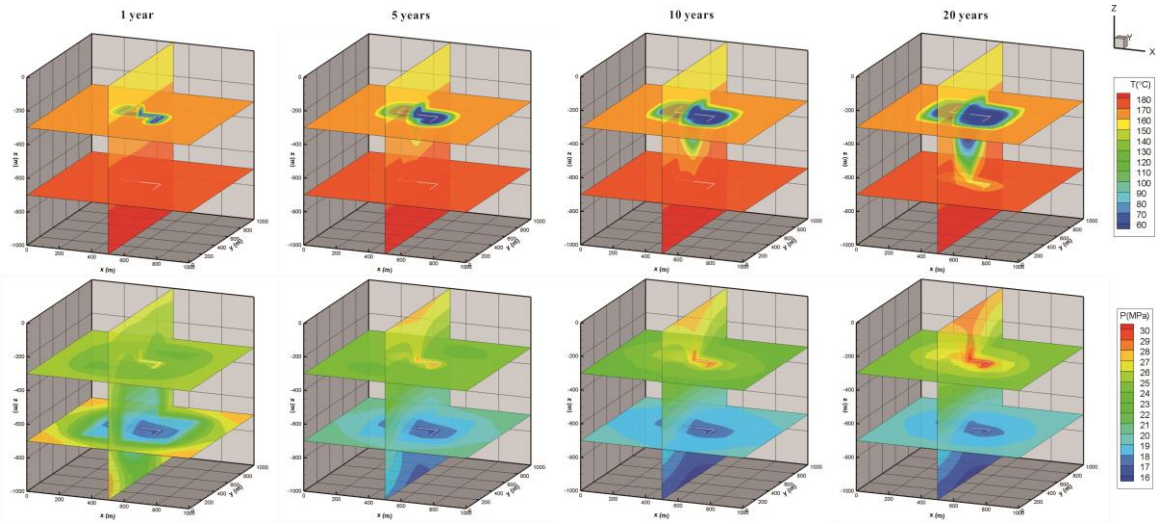

Figure 6: Reservoir temperature contours (first row) and pressure contours (second row) of the base multilateral horizontal well.

3.2 Heat production and electricity generation

According to Eqs. (4) and (5), heat production rate (W_h) and electric power (W_e) are illustrated in Fig. 7. The variation patterns of W_h and W_e are similar to that of T_{pro}. W_h decreases from 25.00 MW to 21.76 MW (reduced by 13.0%), while W_e decreases from 4.35 MW to 3.58 MW (reduced by 17.7%) in the production period of 20 years. For commercial exploitation, the drop of W_e should be less than 15% in the entire production life, and a two-well extraction system should obtain an electric power of higher than 3.5 MW for a water production rate of 50 kg/s [34,36]. Therefore, the geothermal power system proposed in this work can almost meets the commercial requirements.

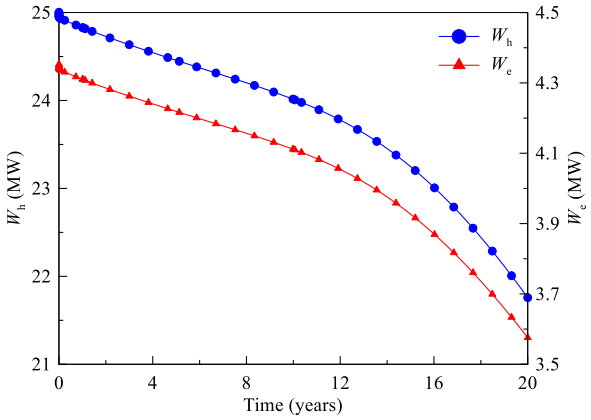

Figure 7: Evolution of output thermal power (W_h) and electric power (W_e)

3.3 Injection pressure and flow impedance

Fig. 8 shows the evolution of injection pressure (P_{inj}) and flow impedance (I_R) during 20 years. The P_{inj} significantly increases from 25.4 to 30.7 MPa. Correspondingly, I_R increases from 0.207 to 0.313 MPa/(kg/s). The slow increase of I_R is mainly caused by the increase of pressure difference and water viscosity , which increases with declining reservoir temperature (Fig. 6). I_R is composed by the inlet impedance near the injection well, the outlet impedance near the production well, and the reservoir impedance [38], which is significantly influenced by water loss, hydro-shearing fracture, and thermal stimulation fracture induced in the production process [35,39]. For an economic EGS project, I_R is expected to be 0.1 - 0.2 MPa/(kg/s) in the entire production life [36,40]. The simulated I_R here is unacceptable. However, the water loss and fracturing effects are not considered in this work, thus the calculated I_R may be slightly higher than in the actual situation.

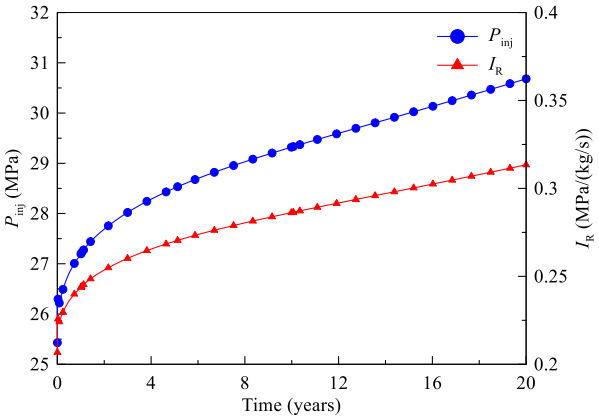

Figure 8: Evolution of injection pressure (P_{inj}) and flow impedance (I_R)

3.4. Energy efficiency

The energy efficiency (η_h) and (η_e) are shown in Fig. 9. During the first year, both η_h and η_e decline drastically due to the significant increase of injection pressure (Fig. 8). During the entire production period, the energy efficiency η_h decreases from 26.1 to 16.5, and η_e decreases from 4.5 to 2.7. The continual decline of energy efficiency indicates that the cost of internal energy consumption increases within operation period. The decrease of energy efficiency is mainly attributed to the decrease of T_{pro} (Fig. 5) and increase of P_{inj} (Fig. 8). An ideal energy efficiency of the two horizontal wells system is within a range of 17.2 - 50.0 [39], the energy efficiency here is 2.7 - 4.5, therefore the designed system cannot meet the industry requirements.

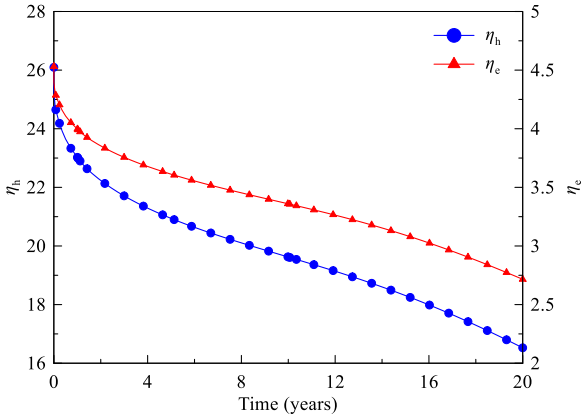

Figure 9: Evolution of heat energy efficiency (η_h) and electric energy efficiency (η_e).

3.5 Economic analysis and environmental benefits

The cost of a geothermal project commonly consists of drilling cost, costs for surface installation, and costs for operation and maintenance.

The drilling costs for the multilateral horizontal well system can be calculated as [41].

$$C = H_v \times P_v + H_h \times P_h \tag{10}$$

where H_v = 3650 m, H_h = 1000 m, P_v = $ 1100 and P_h = $ 3300 [42]. Thus, the total drilling costs are expected to be $ 7.315 million.

The investment costs for surface installation are generally considered to be linear with the size of the power plant. The unit capital cost is supposed to decline exponentially with the increasing plant capacity [24,43]. In this work, the unit capital cost is assumed to be 2000 $/kW according to the design capacity of the proposed EGS power plant [42,43]. Thus, the total costs for surface installation is about $ 7.0 million.

The costs for operation and maintenance include internal energy consumption W_p and other costs like personnel and insurances. The total energy consumed by the two pumps can be calculated from Eqs. (7) and (8). Fig. 10 shows the evolution of W_p and γ_p of two pumps. The total energy consumed by the two pumps is approximately 212.84 GWh. Because the electricity price (industrial electricity price of Qinghai Province in 2016) is 0.05 $/kWh, thus, the estimated costs of internal energy consumption are $ 10.642 million. Considering other costs are about $ 2.0 million [24], the total operation and maintenance costs are expected to be $ 12.642 million.

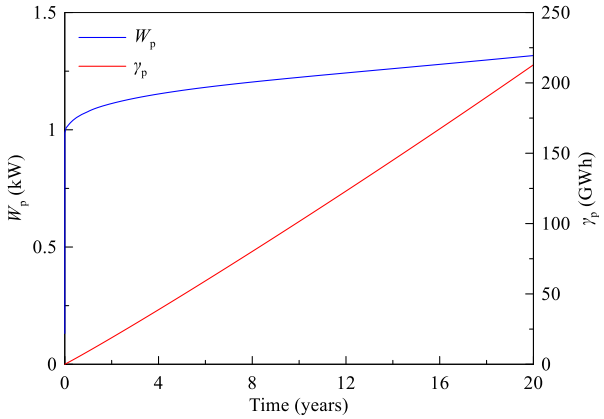

Figure 10: Evolution of internal energy consumption (W_p) and the accumulated energy consumption of pumps (γ_p).

According to the above calculations, the total costs of the proposed multilateral horizontal well system of EGS are estimated at about $ 26.957 million. The modeling results indicate that W_e decreases from 4.35 MW to 3.58 MW during 20 years. Therefore, for the proposed EGS project, a power plant capacity of 3.5 MW is reasonable. As a consequence, the base case can generate approximately 613.20 GWh of electricity during 20 years. The levelized cost of energy (LCOE) is calculated by dividing the total costs by the total power generation, which is estimated at about 0.044 $/kWh and is lower than the industrial electricity price of Qinghai Province in 2016.

Electricity generation from geothermal resources involves much lower greenhouse gas (GHG) emissions than that from fossil fuels [44,45]. The average GHG emissions of the geothermal power plant are approximately 122 g/kWh [44]. For power generation from fossil fuels, the GHG emissions equivalent estimated by International Atomic Energy Agency (IAEA) is equivalent to 460 - 1290 g/kWh [24]. Thus, the reduction of GHG emissions is 338 - 1168 g/kWh for geothermal power plants. Based on the proposed EGS power plant, the results suggest that the total saving in GHG in 20 years are within the range of 0.21 - 0.72 Mt. In terms of carbon emission trading prices, the price of the Beijing pilot in 2018 is basically stable at 55–60 RMB/t [46]. Thus, the estimated profits of total saved GHG are 11.55 - 43.2 million RMB. Therefore, under the global background of carbon neutrality, the proposed EGS power plant is a promising development scheme.

4. DISCUSSION

4.1 Comparisons of base case and cases of classic double-well EGS

In this section, the heat extraction performance of the base case and several classic double-well EGS are compared. Fig. 11. depicts the evolution of T_{pro}, W_e, I_R, η_e of the base case and the cases of classic double-well EGS. As shown in Fig. 11a, the production temperature (T_{pro}) of the horizontal well (Cases 1 and 2) decrease gradually with time, while T_{pro} of vertical well (Case 3) slightly increases in the first 10 years and then declines with time. Meanwhile, T_{pro} of the base case is higher than that of the Case 3. It can be observed that the temperature drop of Case 1 occurred earlier than that of the base case, because of the reduction of the heat transfer area due to the short wellbore length. The temperature curve of the base case is consistent with that of Case 2 owing to the same total well length. The evolution pattern of the electric power is similar to that of the production temperature (Fig. 11b). Fig. 11c show that the I_R of the vertical well case is much lower than that of the horizontal well cases. This is because the production and injection wells are located at the same formation depth, thus the pump work required to overcome the formation pressure is saved, resulting in a smaller injection-production pressure difference and lower flow impedance (Fig. 12). I_R of Case 1 is the highest due to the shortest total well length. The shorter the wellbore length, the smaller the area of water cross section, the same flow rate requires a larger injection-production pressure difference, which results in higher I_R (Fig. 12). The η_e shows the total opposite situation compared to I_R (Fig. 11d), this indicates that the energy efficiency is mainly dependent on the internal energy consumption.

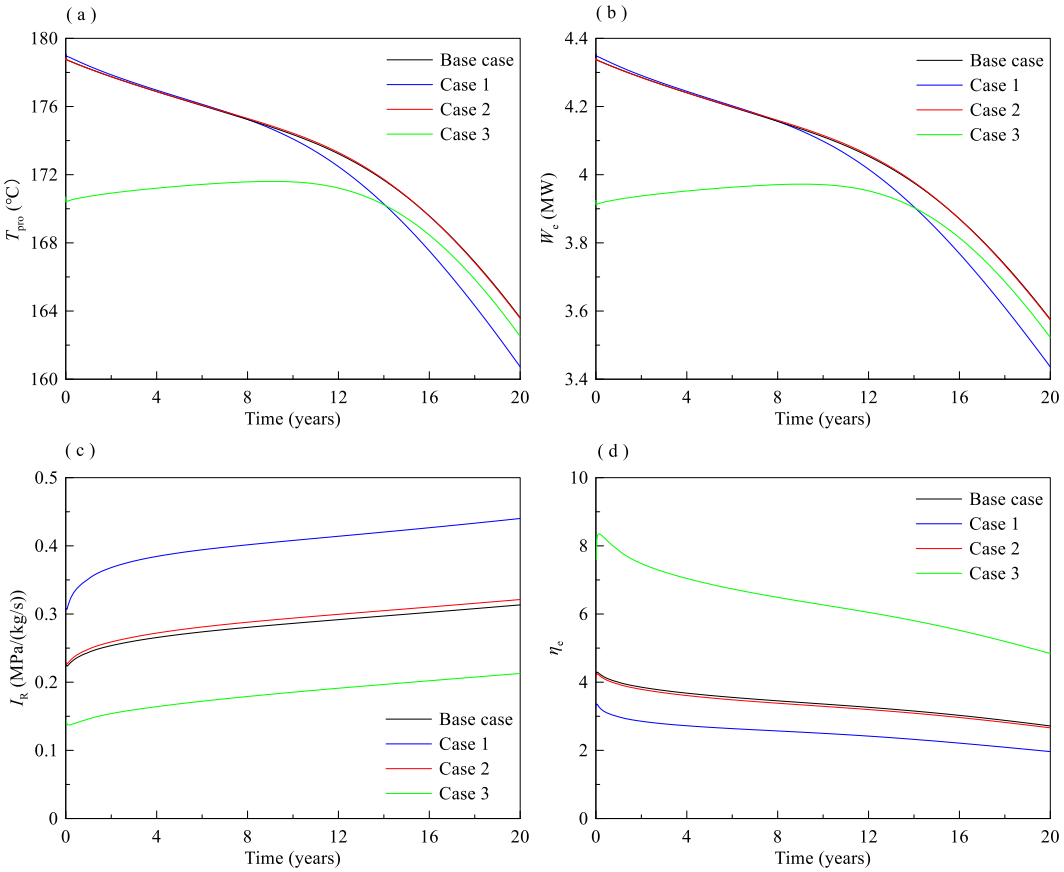

Figure 11: Comparison of base case and classic double-wells of various performance parameters. (a) production temperature T_{pro}, (b) electric power W_e, (c) flow impedance I_R, and (d) energy efficiency η_e.

Fig. 12. shows the spatial distribution of reservoir temperature and pressure for the base case and classic double-well cases after 20 years. It can be observed that the low-temperature zone extends outward from the injection well to the production well. The heat extraction of SRV in y direction of the base case is being more thorough than Cases 1 and 2. But Case 2 can obtain more heat compensation of surrounding rock due to its proximity to HDR area. A preferential channel along the diagonal plane is formed for the expansion of the low-temperature zone of Case 3. The injection-production pressure difference of horizontal well cases is larger of vertical well case, increasing with the decrease of the wellbore length. Therefore, the largest difference is observed for Case 1. In Case 3, the pressure difference is the smallest due to the production and injection wells are located at the same formation depth, and the pump work required to overcome the formation pressure is saved.

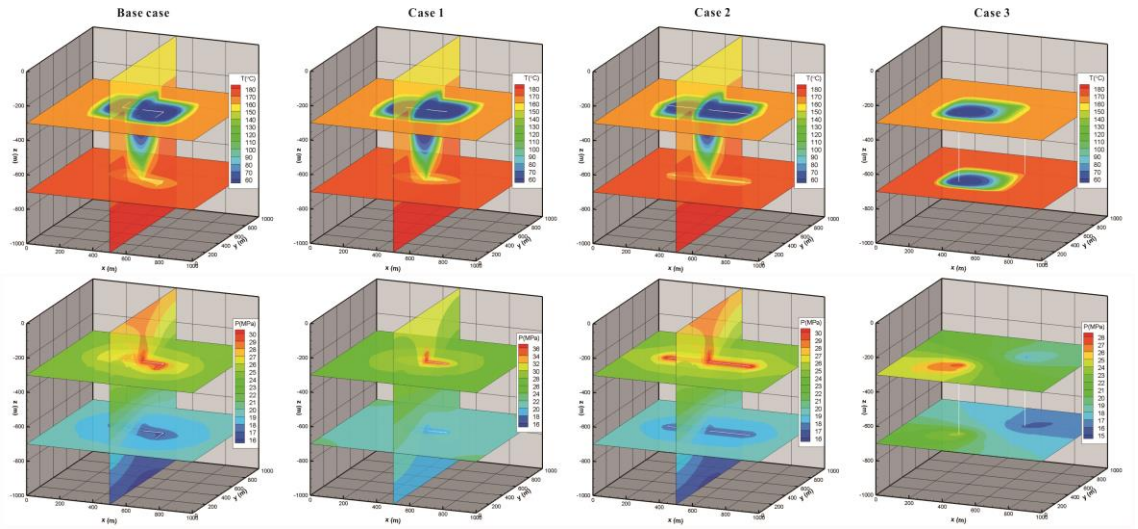

Figure 12: Spatial temperature and pressure distribution after 20 years for different well arrangement.

In conclusion, the multilateral horizontal well EGS has an equal or even higher heat extraction performance than the conventional horizontal and vertical double-well EGS, although the multilateral horizontal well EGS obtain less thermal compensation from the surrounding rock. Meanwhile, the multilateral horizontal well EGS only requires one vertical wellbore, which induces a dramatic reduction of the drilling cost. On the other hand, the arrangements and geometrical parameters of multilateral wells, including the

well number, well length, well diameter, etc., can also be optimized to further improve the heat extraction performance. Therefore, the heat extraction performances of the optimal EGSs with multilateral wells and double wells should be compared in future studies.

4.3 Influence of well horizon

Fig. 13 shows the dependence of T_{pro}, W_e, I_R, and η_e on the horizon of injection and production well. Switching the horizon of the injection and production well has great impact on T_{pro} and W_e (Fig. 13a and b). T_{pro} of LIUP increases gradually with time before 12 years and then declines. This is due to the high temperature of the lower reservoir heats the upward the working fluid. The heat exchange between the fluid and the upper reservoir occurs during the migration of working fluid to the upper production well, which has a heating effect on the upper reservoir. With continues heat extraction, the heat in the deep high temperature reservoir gradually recoveres, and the low-temperature region gradually propagates to the production well. As a result, the T_{pro} and W_e first increases and then decreases. Fig. 13c shows that switching the horizon of the injection and production well results in a drastic decrease of I_R. In LIUP case, the production and injection well horizons are switched based on the base case, the pump work required to overcome the formation pressure is twice saved, resulting in a smaller injection-production pressure difference and lower flow impedance. Switching the well horizon results in the drop of I_R from 0.22 to 0.31 to 0.11 to 0.20 MPa/(kg/s), and η_e increases from 2.7 to 4.5 to 7.7 - 28.3 (Fig. 13d). This is due to the combined effect of the W_e and I_R changes caused by the switch of well horizon, where I_R is more obviously reduced.

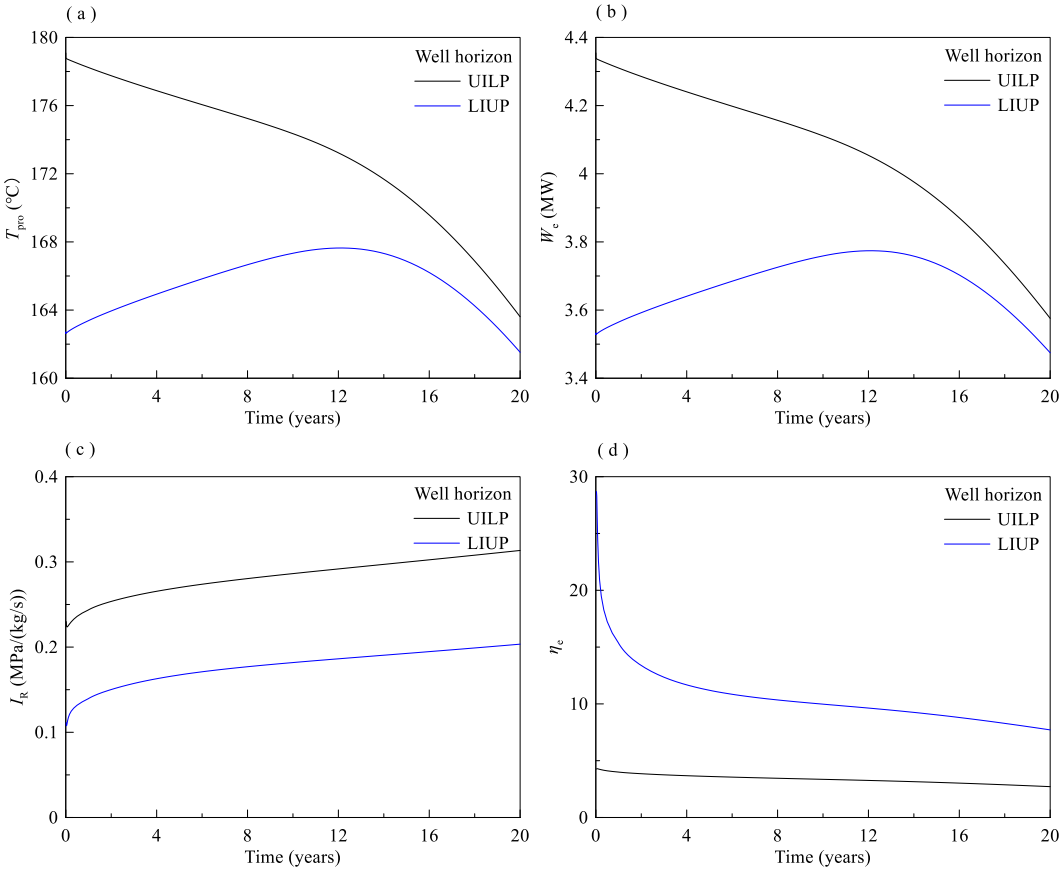

Figure 13: Sensitivity of various performance parameters to well horizon: (a) production temperature T_{pro}, (b) electric power W_e, (c) flow impedance I_R, and (d) energy efficiency η_e.

Fig. 14 depicts the spatial distribution of pressure and temperature after 20 years for the base case and Case 4. It can be observed that the injection and production pressure difference of base case reaches approximately 14 MPa, which is higher than that of 8 MPa of Case 4. For the production well horizon, the low temperature zone of LIUP case after 20 years is smaller due to the production well lays in the upper layer with lower temperature.

Well horizon is a key parameter affecting the EGS performance. The well layout of upper injection and lower production could result in high production temperature but low energy efficiency. While the well layout of lower injection and upper production results in low production temperature, but the temperature range is less than 10 ℃ which is more friendly to the regulation of the ground generation equipment. In addition, the consumption of pump power is greatly reduced, and the energy efficiency is better. Therefore, lower injection upper production well layout is more favorable.

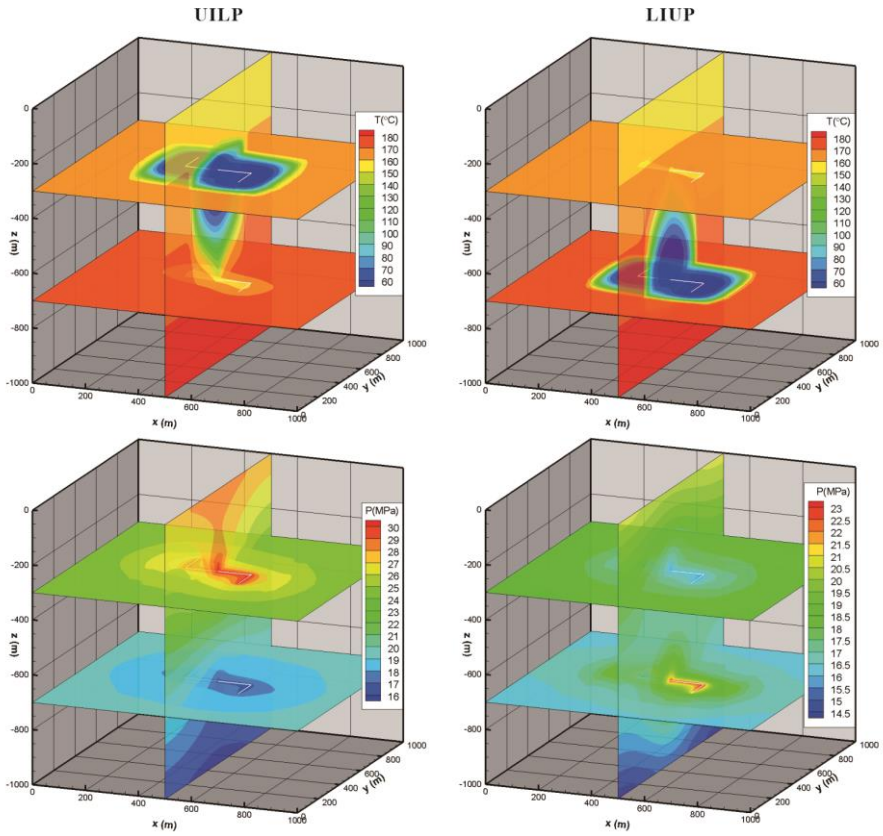

Figure 14: Spatial temperature and pressure distribution after 20 years for different injection-production well horizon.

4.3 Influence of branch number

Fig. 15 shows the dependence of T_{pro}, W_e, I_R, and η_e on branch numbers. Fig. 15a and b shows that the increase of branch number results in a decline of T_{pro} and W_e, with the difference of T_{pro} and W_e mainly occurs in late stage. This is because the increase of branch number leads to a larger well interference and a lower heat exchange area between fluid and rock matrix (Fig. 16). As a consequence, more energy is preserved in the rocks after 20 years production. Compared with the base case of 2 branches, the T_{pro} decreases from 163.6 ℃ to 160.7 ℃ for 6 branches. Fig. 15c show that the increase of branch number results in a slight increase of I_R. This is because the more branches result in the lower water temperature and finally the higher water viscosity. Fig. 15b shows increasing branch number from 2 to 6 results in a drop of W_e from 4.35 - 3.58 MW to 4.35 - 3.43 MW. Similarly, branch number has a negative influences on η_e (Fig. 15d).

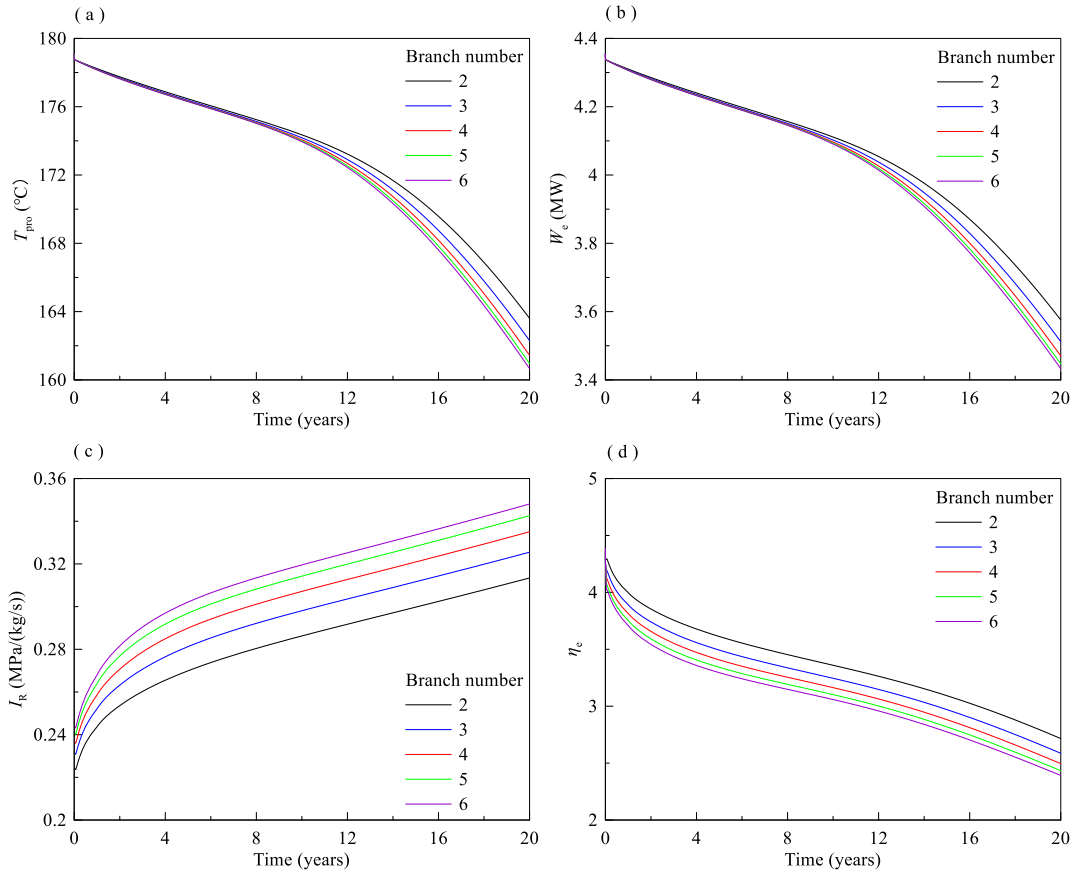

Figure 15: Sensitivity of various performance parameters to branch number : (a) production temperature T_{pro}, (b) electric power W_e, (c) flow impedance I_R, and (d) energy efficiency η_e.

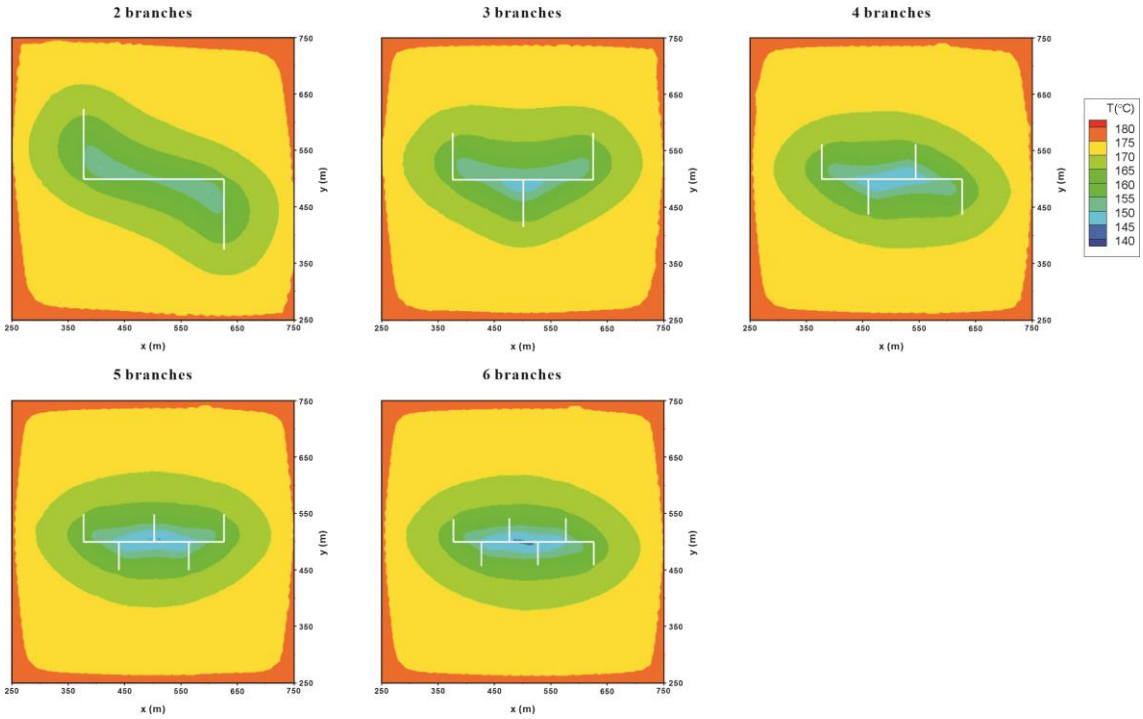

Figure 16: Spatial distribution of SRV temperature of production well horizon after 20 years for different branch number

Overall, branch number is a key parameter affecting the EGS performance. Under the same total well length, the less branch number can effectively improve water production temperature and heat production rate. It should be noted that the current discussion is based on the condition that the total well length is constant. If the main wellbore length and the length of a single branch well are fixed, the impact of branch number on productivity remains to be discussed. Branch number may have a positive impact on production capacity, however the drilling cost will be increased correspondingly. The overall economics are uncertain, and this is an issue that needs further study in the future.

4.4 Influence of branch spacing

Fig. 17 shows the dependence of T_{pro}, W_e, I_R, and η_e on branch spacing (d_b). Fig. 17a and b shows that the decrease of branch spacing results in a decline of T_{pro} and W_e. The T_{pro} and W_e of the two cases which the d_b is reduced basically coincide due to well interference (Fig. 18). Compared with the base case, the T_{pro} decreases from 163.6 ℃ to 160.5 ℃ for the 0 m d_b. Fig. 17c shows that the decrease of d_b results in an increase of I_R. Furthermore, decreasing d_b from 250 m to 0 m results in a drop of W_e from 4.35 - 3.58 MW to 4.35 - 3.43 MW (Fig. 17b), and it also has a negative influence on η_e (Fig. 17d).

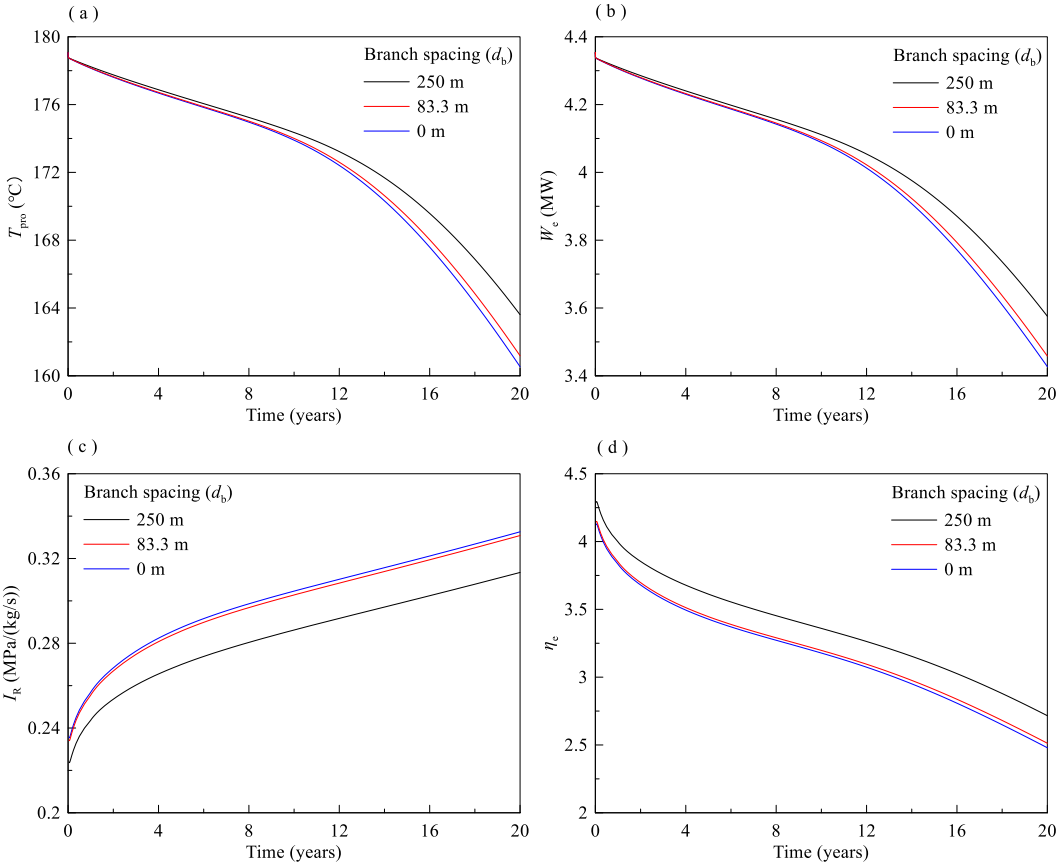

Figure 17: Sensitivity of various performance parameters to branch spacing : (a) production temperature T_{pro}, (b) electric power W_e, (c) flow impedance I_R, and (d) energy efficiency η_e.

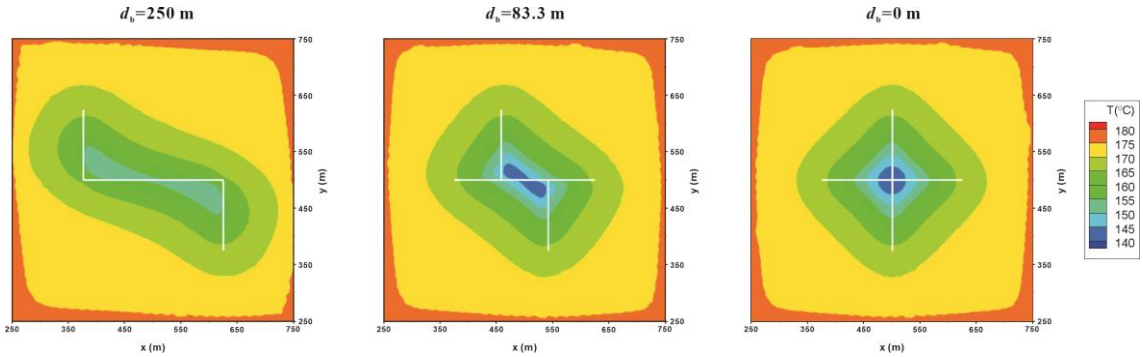

Figure 18: Spatial distribution of SRV temperature of production well horizon after 20 years for different branch spacing

From above discussion, branch spacing has little effect on EGS performance. It should be noted that the current discussion is based on the condition that there are only 2 branch wells and they are arranged in the direction of cross side of the main wellbore. The well interference is mainly between the branch well and the main well. When increasing the branch number, more than one branch will be set on the same side of the main well. Consequently, the branch interference is enhanced. The impact of branch spacing on productivity remains to be discussed.

4.5 Influence of permeability of SRV

Fig. 19 shows the dependence of T_{pro}, W_e, I_R, and η_e on the permeability of SRV (k_{SRV}). The T_{pro} and W_e decreases with the increase of permeability of SRV. The T_{pro} and W_e decrease more for decreasing k_{SRV} from the 1×10^{-15} m^2 to 5×10^{-15} m^2, while a minor decrease for decreasing the k_{SRV} from 5×10^{-15} m^2 to 1×10^{-14} m^2. Furthermore, the T_{pro} and W_e in the first 12 years is similar for k_{SRV} of 5×10^{-15} m^2 and 5×10^{-14} m^2, while a higher T_{pro} and W_e in the following 8 years is observed for k_{SRV} of 5×10^{-14} m^2.. Fig. 19c

shows that increase of k_{SRV} results in a drastic decrease of I_R. Increasing k_{SRV} from 5×10^{-15} m^2 to 5×10^{-14} m^2 results in the drop of I_R from 0.22 - 0.31 to 0.09 - 0.10 MPa/(kg/s), and correspondingly the η_e increases from 2.7 - 4.5 to 6.2 - 7.9 (Fig. 19d). On the contrary, the decrease of permeability lower than 5×10^{-15} m^2 results in a drastic increase of I_R and a drastic decrease of η_e.

This suggests that permeability change means a fluid flow condition change which results in the change of flow impedance. Due to the geothermal gradient, the change of flow impedance will change the proportion of upper cold fluid and lower hot fluid entering the production well, resulting in the change of production temperature. Meanwhile, the thermal exploitation is more sufficient in higher permeability reservoir, especially the surrounding regions (Fig. 20), and the temperature drop rate of production temperature slows down in the later stage of thermal exploitation.

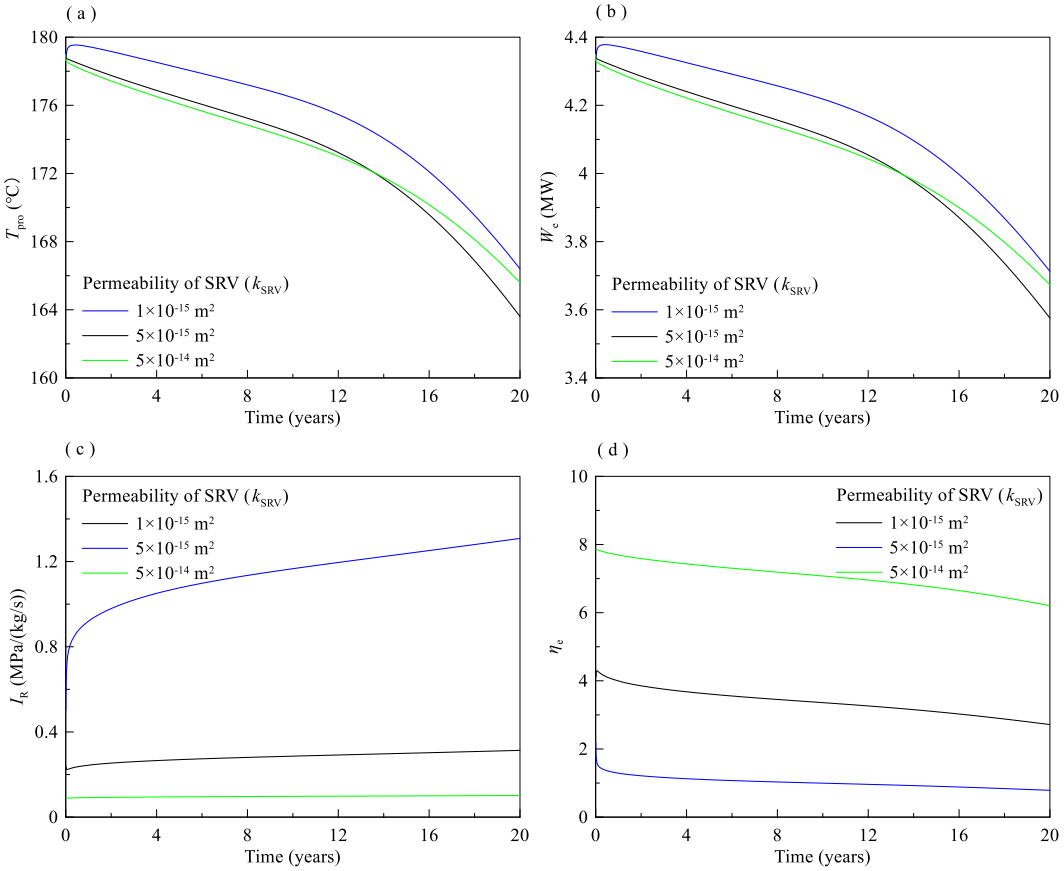

Figure 19: Sensitivity of various performance parameters to the permeability of SRV : (a) production temperature T_{pro}, (b) electric power W_e, (c) flow impedance I_R, and (d) energy efficiency η_e

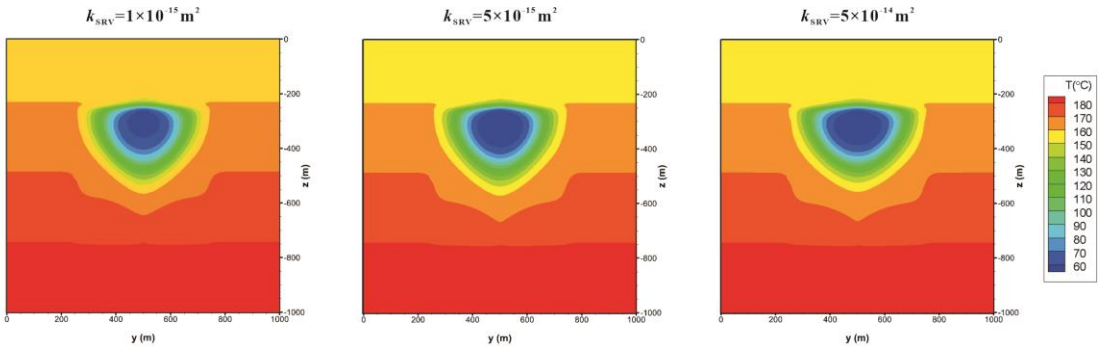

Figure 20: Spatial distribution of fluid temperature after 10 years for different SRV permeability

The higher k_{SRV} is a necessary condition to reduce flow impedance and to save energy consumption. Actually, k_{SRV} is fundamentally determined by fracture aperture. When the production pressure P_{pro} is lower than the fracture extension stress, the fracture aperture near the production well is maintained at constant with a minimum value, which is supported by the wall of rough fractures. Thus, the potential methods for increasing fracture permeability is pressure propping by holding an elevated back-pressure in the production well [24, 36, 39].

High permeability of the reservoir can reduce flow impedance and save pump energy consumption, while low permeability will lead to high pump costs and even the failure of injection. Considering the low porosity and permeability of HDR reservoir, it is difficult to stimulate the reservoir and predict the stimulation results. The development of fractures is closely related to natural faults and

stimulation means, and the thermal reservoir after stimulation presents strong heterogeneity. At this time, the application of multilateral well system based on the permeability distribution characteristics of the reservoir, can enhance the reservoir connectivity while avoiding fluid short-circuits, which is more conducive to the economic and efficient exploitation of heat from the reservoir.

5. CONCLUSIONS

Based on the GR1 borehole of the Qiabuqia geothermal area, Gonghe Basin, a three-dimensional multilateral horizontal well reservoir model is set up to evaluate the extraction potential of the 2650-3650 m granitic HDR reservoir. The production characteristics of the novel well system are investigated. Subsequently, the heat extraction performance of multilateral horizontal well and several classic double wells are compared. The sensitivity of production criteria to the well horizon, branch number, branch spacing, and permeability of SRV are systematically and quantitatively compared. Based on the simulation results, the following conclusions can be drawn:

(1) For the basic multilateral horizontal well system, the initial production temperature and electric power reaches 178.4 ℃ and 4.35 MW and decreases by 8.3% and 17.7% during 20 years production, respectively, which satisfy the commercial standard of EGS development.

(2) The basic multilateral horizontal well system attains an electric power of 3.58 - 4.35 MW, a flow impedance of 0.207 - 0.313 MPa/(kg/s), and an electric energy efficiency of 2.7- 4.5 in the period of 20 years.

(3) The installed power capacity of the proposed configuration is 3.5MW based on the simulation results. The designed power plant can generate approximately 613.20 GWh of electricity and the total costs are expected to be $ 26.957 million. The LCOE in this work is estimated at 0.044 $/kWh, which is lower than the industrial electricity price of Qinghai Province in 2016. The saving in GHG emissions is between 0.21 - 0.72 Mt over 20 years, and the estimated profits are 11.55 - 43.2 million RMB.

(4) The multilateral horizontal well EGS had higher production temperature and electric power than the configurations of horizontal non-branch well and conventional vertical double-well EGS. However, the vertical double-well EGS could obtain smaller flow impedance. But the multilateral horizontal well EGS only required one vertical wellbore, which could dramatically save the drilling cost.

(5) The heat production performance of geothermal reservoir highly depends on the well horizon and branch well arrangement. The layout of upper injection and lower production wells could result in high production temperature but low energy efficiency. While the layout of lower injection and upper production wells results in low production temperature but high energy efficiency. Layout of a lower injection and a upper production well is more favorable. A large number of branch wells brings larger flow impedance and lower production temperature, due to the strong well interference. Therefore, under the same total well length, less branches and large branch spacing is the basic principle for the design of multilateral horizontal well system.

(6) Reservoir permeability is one of the main parameters affecting flow impedance and energy efficiency. The higher permeability can effectively reduce flow impedance and save internal energy consumption.

The proposed EGS with multilateral horizontal wells is demonstrated as an effective method to exploit the HDR reservoir of the Qiabuqia geothermal area. The presented numerical model also offered an efficient tool for the optimization and design of the EGS with multilateral horizontal wells. For homogeneous reservoir, the advantage of multilateral horizontal well system is minor compared to classic horizontal double well system with same total well length. However, for heterogeneous reservoir, based on the permeability distribution characteristics of the reservoir, the application of multilateral well system can enhance the connectivity while avoiding fluid short-circuits, which is more conducive to the economic and efficient geothermal development. Therefore, the influence of reservoir heterogeneity and the existence of natural faults and the artificial fractures could be further discussed to optimize the heat extraction performance in our future studies.

REFERENCES

[1] B. Zheng, J. Xu, T. Ni, M. Li, Geothermal energy utilization trends from a technological paradigm perspective, Renewable Energy. 77 (2015) 430-441.

[2] J.Y. Wang, S.B. Hu, Z.H. Pang, L.J. He, P. Zhao, C.Q. Zhu, S. Rao, X.Y. Tang, Y.L. Kong, L. Luo, Estimate of geothermal resources potential for hot dry rock in the continental area of China, Sci. Technol. Rev. 30 (32) (2012) 25-31.

[3] K. Breede, K. Dzebisashvili, X. Liu, G. Falcone, A systematic review of enhanced (or engineered) geothermal systems: past, present and future, Geoth. Energy 1 (1) (2013) 4.

[4] M.Z. Lukawski, R.L. Silverman, J.W. Tester, Uncertainty analysis of geothermal well drilling and completion costs, Geothermics. 64 (2016) 382-91.

[5] Y. Zeng, J. Zhan, N. Wu, Y. Luo, W. Cai, Numerical investigation of electricity generation potential from fractured granite reservoir by water circulating through three horizontal wells at Yangbajing geothermal field, Applied Thermal Engineering. 104 (2016) 1-15.

[6] S.D. Cinelli, A.H. Kamel, Novel Technique to Drill Horizontal Laterals Revitalizes Aging Field. SPEIADC Drill. Conf., Amsterdam, The Netherlands: Society of Petroleum Engineers, 2013.

[7] X. Song, Y. Shi, G. Li, R. Yang, G. Wang, R. Zheng, J. Li, Z. Lyu, Numerical simulation of heat extraction performance in enhanced geothermal system with multilateral wells, Appl Energy. 218 (2018) 325-37.

[8] H. Wang, J. Guo, L. Zhang, A semi-analytical model for multilateral horizontal wells in low-permeability naturally fractured reservoirs, J Pet Sci Eng. 149 (2017) 564-78.

[9] B. Sobhaniaragh, J. Trevelyan, W.J. Mansur, F.C. Peters, Numerical simulation of MZF design with non-planar hydraulic fracturing from multi-lateral horizontal wells, J Nat Gas Sci Eng. 46 (2017) 93-107.

[10] X. Ren, L. Zhou, J. Zhou, Z. Lu, X. Su, Numerical analysis of heat extraction efficiency in a multilateral-well enhanced geothermal system considering hydraulic fracture propagation and configuration, Geothermics. 87 (2020) 101834.

[11] P. Mao, Y. Wan, J. Sun, Y. Li, G. Hu, F. Ning, N. Wu, Numerical study of gas production from fine-grained hydrate reservoirs using a multilateral horizontal well system, Applied Energy. 301 (2021) 117450.

[12] A.M.S. Ragab, Radial drilling technique for improving well productivity in PetrobelEgypt. North Africa Technical Conference and Exhibition. Society of Petroleum Engineers, 2013.

[13] S.D. Cinelli, A.H. Kamel, Novel technique to drill horizontal laterals revitalizes aging field. SPE/IADC Drilling Conference. Society of Petroleum Engineers, 2013.

[14] R. Nair, E. Peters, S. Šliaupa, R. Valickas, S. Petrauskas, A case study of radial jetting technology for enhancing geothermal energy systems at Klaipėda geothermal demonstration plant. 42nd workshop on Geothermal Reservoir Engineering, Stanford University, February 13–15; 2017. p. 1–11.

[15] C.G. Wang, Y.S. Lv, Gonghe Basin: a new and worth-researching basin, Xinjing Pet. Geol. 25 (5) (2004) 471-473.

[16] C. Zhang, S.S. Zhang, S.T. Li, X.F. Jia, G.Z. Jiang, P. Gao, Y.B. Wang, S.B. Hu, The characteristics of geothermal field of the Qiabuqia geothermal area in the Gonghe basin, northeastern Tibetan Plateau, Chin. J. Geophys. (2018) 1-12.

[17] C. Zhang, G. Jiang, Y. Shi, Z. Wang, Y. Wang, S. Li, X. Jia, S. Hu, Terrestrial heat flow and rustal thermal structure of the Gonghe-Guide area, northeastern Qinghai-Tibetan plateau, Geothermics 72 (2018) 182-192.

[18] E.C. Bullard, The time necessary for a bore hole to attain temperature equilibrium, Geophys. J. Int. 5 (s5) (1947) 127-130.

[19] L.J. He, S.B. Hu, S.P. Huang, W.C. Yang, J.Y. Wang, Y.S. Yuan, S.C. Yang, Heat flow study at the Chinese Continental Scientific Drilling site: borehole temperature, thermal conductivity, and radiogenic heat production, J. Geophys. Res.: Solid Earth 113 (B2) (2008) 1-16.

[20] G.T. Pan, Q.H. Xiao, S.N. Lu, F.J. Den, Y.M. Feng, K.X. Zhang, Z.Y. Zhang, F.G. Wang, G.F. Xing, G.J. Hao, X.F. Feng, Subdivision of tectonic units in China, Geol. China 36 (2009) 1-28.

[21] J. Andaverde, S.P. Verma, E. Santoyo, Uncertainty estimates of static formation temperatures in boreholes and evaluation of regression models, Geophys. J. Roy. Astron. Soc. 160 (3) (2005) 1112-1122.

[22] W.D. Yan, Y.X. Wang, X.Z. Gao, S.H. Zhang, Y.H. Ma, X.G. Shang, S.Y. Guo, Distribution and aggregation mechanism of geothermal energy in Gonghe basin, Northwest. Geol. 46 (4) (2013) 223-230.

[23] G. F. Yue, X.F. Deng, L.X. Xing, W.J. Lin, F. Liu, Y.G. Liu, G.L. Wang, Numerical simulation of hot dry rock exploitation using enhanced geothermal systems in Gonghe Basin, Science & Technology Review. 33(19) (2015) 62-67.

[24] T. Xu, Y. Yuan, X. Jia, Y. Lei, S. Li, B. Feng, Z. Hou, Z. Jiang, Prospects of power generation from an enhanced geothermal system by water circulation through two horizontal wells: A case study in the Gonghe Basin, Qinghai Province China, Energy. 148 (2018) 196-207.

[25] C. Zhang, G. Jiang, X. Jia, S. Li, S. Zhang, D. Hu, S. Hu, Y. Wang, Parametric study of the production performance of an enhanced geothermal system: a case study at the Qiabuqia geothermal area, northeast Tibetan plateau, Renewable Energy. 132 (2019) 959-978.

[26] J. Zhang, J. Xie, H. Zhang, Production capacity and mining plan optimization of fault/fracture-controlled EGS model in Gonghe Basin, Energy Sci Eng. 7 (2019) 2966-2983. https://doi.org/10.1002/ese3.473

[27] K. Pruess, C. Oldenburg, G. Moridis, TOUGH2 User's Guide, Version 2.0.; Lawrence Berkeley National Laboratory: Berkeley, CA, USA, 1999.

[28] Y.A. Popov, F.C.P. Dan, J.H. Sass, C.F. Williams, H. Burkhardt, Characterization of rock thermal conductivity by high-resolution optical scanning, Geothermics. 28 (2) (1999) 253-276.

[29] Y.Q. Zhuang, C.H. Zhang, M.C. Zhu, Y.Q. Zhu, J. Luo, Q.H. Guo, Laboratory study of improving granite permeability by using mud acid as the chemical stimulus, Saf. Environ. Eng. 24 (2) (2017) 16-21.

[30] G.F. Yue, X.F. Deng, L. Xing, W.J. Lin, F. Liu, Y.G. Liu, G.L. Wang, Numerical simulation of hot dry rock exploitation using enhanced geothermal systems in Gonghe Basin, Sci. Technol. Rev. 33 (19) (2015) 62-67.

[31] K. Evans, Enhanced/engineered geothermal system: an introduction with overviews of deep systems built and circulated to date. In Proceedings of the China Geothermal Development Forum, Beijing, 2010. pp. 395-418.

[32] S.K. Sanyal, S.J. Butler, An analysis of power generation prospects from enhanced geothermal systems, Geotherm. Resour. Counc. Trans. 29 (2005) 1-6.

[33] B. Liu, H. Jin, L. Sun, Z. Sun, Z. Su, C. Zhang, Holocene climatic change revealed by aeolian deposits from the Gonghe Basin, northeastern Qinghai-Tibetan Plateau, Quat Int. 296 (2013) 231-40. https://doi.org/10.1016/j.quaint.2012.05.003.

[34] S.K. Sanyal, S.J. Butler, An analysis of power generation prospects from enhanced geothermal systems. Geotherm. Resour. Counc. Trans. 29 (2005) 131-8.

[35] J.W. Tester, B.J. Anderson, A.S. Batchelor, D.D. Blackwell, R. DiPippo, The future of geothermal energy - impact of enhanced geothermal systems (EGS) on the United States in the 21st century. MIT - Massachusetts Inst Technol, 2006.

[36] Y.C. Zeng, J.M. Zhan, N.Y. Wu, Y.Y. Luo, W.H. Cai, Numerical simulation of electricity generation potential from fractured granite reservoir through vertical wells at Yangbajing geothermal field, Energy. 103 (2016) 290-304. https://doi.org/10.1016/j.energy.2016.02.123.

[37] J.D. Garnish, Hot dry rock - a european perspective. Geotherm Resour Counc Trans. 9 (1985) 329-37.

[38] H. Murphy, D. Brown, R. Jung, I. Matsunaga, R. Parker, Hydraulics and well testing of engineered geothermal reservoirs, Geothermics. 28 (1999) 491-506. https://doi.org/10.1016/S0375-6505(99)00025-5.

[39] Y.C. Zeng, Z. Su, N.Y. Wu, Numerical simulation of heat production potential from hot dry rock by water circulating through two horizontal wells at Desert Peak geothermal field, Energy. 56 (2013) 56: 92-107.https://doi.org/10.1016/j.energy.2013.04.055.

[40] Y.C. Zeng, N.Y. Wu, Z. Su, X.X. Wang, J. Hu, Numerical simulation of heat production potential from hot dry rock by water circulating through a novel single vertical fracture at Desert Peak geothermal field, Energy. 63 (2013) 268-82.https://doi.org/10.1016/j.energy.2013.10.036.

[41] Z. Feng, Y. Zhao, A. Zhou, N. Zhang, Development program of hot dry rock geothermal resource in the Yangbajing Basin of China, Renew Energy. 39 (2012) 490-495. https://doi.org/10.1016/j.renene.2011.09.005.

[42] Y. Zhang, Z. Li, L. Guo, P. Gao, X. Jin, T. Xu, Electricity generation from enhanced geothermal systems by oilfield produced water circulating through reservoir stimulated by staged fracturing technology for horizontal wells: a case study in Xujiaweizi area in Daqing Oilfield. China, Energy. 78 (2014) 788-805.

[43] C.R. Chamorro, M.E. Mondejar, R. Ramos, J.J. Segovia, M.C. Martín, M.A. Villamanan, World geothermal power production status: energy, environmental and economic study of high enthalpy technologies, Energy. 42 (2012) 10-8. https://doi.org/10.1016/j.energy.2011.06.005.

[44] R. Bertani, I Thain, Geothermal power generating plant CO2 emission survey, IGA News. 49 (2002) 1-3.

[45] H. Kristmannsdottir, H. Armannsson, Environmental aspects of geothermal energy utilization, Geothermics. 32 (2003) 451-61. https://doi.org/10.1016/S0375-6505(03)00052-X.

[46] Y. Yin, Z. Jiang, Y. Liu, Z. Yu, Factors Affecting Carbon Emission Trading Price: Evidence from China, Emerging Markets Finance and Trade. 55 (2019) 3433-3451.